Analysis of an electro-optic modulator based on a graphene-silicon hybrid 1D photonic crystal nanobeam cavity

Ting Pan,[1] Ciyuan Qiu,[1,*] Jiayang Wu,[1] Xinhong Jiang,[1] Boyu Liu,[1] Yuxing Yang,[1] Huanying Zhou,[1] Richard Soref,[2] and Yikai Su[1]

[1]*State Key Lab of Advanced Optical Communication Systems and Networks, Department of Electronic Engineering, Shanghai Jiao Tong University, Shanghai 200240, China*

[2]*The Engineering Program, University of Massachusetts, Boston, Massachusetts 02125, USA*

**qiuciyuan@sjtu.edu.cn*

Abstract: We propose and numerically study an on-chip graphene-silicon hybrid electro-optic (EO) modulator operating at the telecommunication band, which is implemented by a compact 1D photonic crystal nanobeam (PCN) cavity coupled to a bus waveguide with a graphene sheet on top. Through electrically tuning the Fermi level of the graphene, both the quality factor and the resonance wavelength can be significantly changed, thus the in-plane lightwave can be efficiently modulated. Based on finite-difference time-domain (FDTD) simulation results, the proposed modulator can provide a large free spectral range (FSR) of 125.6 nm, a high modulation speed of 133 GHz, and a large modulation depth of ~12.5 dB in a small modal volume, promising a high performance EO modulator for wavelength-division multiplexed (WDM) optical communication systems.

OCIS codes: (230.2090) Electro-optical devices; (160.5298) Photonic crystals; (230.4110) Modulators; (230.7400) Waveguides, slab.

References and links

1. A. V. Krishnamoorthy, R. Ho, X. Z. Zheng, H. Schwetman, J. Lexau, P. Koka, G. L. Li, I. Shubin, and J. E. Cunningham, "Computer systems based on silicon photonic interconnects," Proc. IEEE **97**(7), 1337–1361 (2009).
2. R. Soref, "The past, present, and future of silicon photonics," IEEE J. Sel. Top Quantum Electron. **12**(6), 1678–1687 (2006).
3. R. A. Soref and B. R. Bennett, "Electrooptical effects in silicon," IEEE J. Quantum Electron. **23**(1), 123–129 (1987).
4. K. I. Bolotin, K. J. Sikes, Z. Jiang, M. Klima, G. Fudenberg, J. Hone, P. Kim, and H. L. Stormer, "Ultrahigh electron mobility in suspended graphene," Solid State Commun. **146**(9-10), 351–355 (2008).
5. K. F. Mak, M. Y. Sfeir, Y. Wu, C. H. Lui, J. A. Misewich, and T. F. Heinz, "Measurement of the optical conductivity of graphene," Phys. Rev. Lett. **101**(19), 196405 (2008).
6. M. Liu, X. Yin, E. Ulin-Avila, B. Geng, T. Zentgraf, L. Ju, F. Wang, and X. Zhang, "A graphene-based broadband optical modulator," Nature **474**(7349), 64–67 (2011).
7. M. Liu, X. Yin, and X. Zhang, "Double-layer graphene optical modulator," Nano Lett. **12**(3), 1482–1485 (2012).
8. C. Qiu, W. Gao, R. Vajtai, P. M. Ajayan, J. Kono, and Q. Xu, "Efficient modulation of 1.55 μm radiation with gated graphene on a silicon microring resonator," Nano Lett. **14**(12), 6811–6815 (2014).
9. W. Du, E. P. Li, and R. Hao, "Tunability analysis of a graphene-embedded ring modulator," IEEE Photonics Technol. Lett. **26**(20), 2008–2011 (2014).
10. Q. Xu, B. Schmidt, J. Shakya, and M. Lipson, "Cascaded silicon micro-ring modulators for WDM optical interconnection," Opt. Express **14**(20), 9431–9435 (2006).
11. Q. Xu, D. Fattal, and R. G. Beausoleil, "Silicon microring resonators with 1.5-μm radius," Opt. Express **16**(6), 4309–4315 (2008).
12. P. B. Deotare, M. W. McCutcheon, I. W. Frank, M. Khan, and M. Loncar, "High quality factor photonic crystal nanobeam cavities," Appl. Phys. Lett. **94**(12), 121106 (2009).
13. Q. Quan and M. Loncar, "Deterministic design of wavelength scale, ultra-high Q photonic crystal nanobeam cavities," Opt. Express **19**(19), 18529–18542 (2011).
14. J. Hendrickson, R. Soref, J. Sweet, and W. Buchwald, "Ultrasensitive silicon photonic-crystal nanobeam electro-optical modulator: design and simulation," Opt. Express **22**(3), 3271–3283 (2014).

#242279 Received 8 Jun 2015; revised 31 Jul 2015; accepted 31 Jul 2015; published 27 Aug 2015

15. W. S. Fegadolli, J. E. B. Oliveira, V. R. Almeida, and A. Scherer, "Compact and low power consumption tunable photonic crystal nanobeam cavity," Opt. Express **21**(3), 3861–3871 (2013).
16. R. Hao, W. Du, H. S. Chen, X. F. Jin, L. Z. Yang, and E. P. Li, "Ultra-compact optical modulator by graphene induced electro-refraction effect," Appl. Phys. Lett. **103**(6), 061116 (2013).
17. W. Gao, J. Shu, C. Qiu, and Q. Xu, "Excitation of plasmonic waves in graphene by guided-mode resonances," ACS Nano **6**(9), 7806–7813 (2012).
18. J. Kim, H. Son, D. J. Cho, B. Geng, W. Regan, S. Shi, K. Kim, A. Zettl, Y. R. Shen, and F. Wang, "Electrical control of optical plasmon resonance with graphene," Nano Lett. **12**(11), 5598–5602 (2012).
19. S. Shen, K. Wu, L. Sun, and C. Jiang, "Theoretical study of graphene-silicon nitride-silicon hybrid photonic crystal waveguides for four-wave mixing enhancement," Appl. Opt. **54**(12), 3640–3644 (2015).
20. A. Majumdar, J. Kim, J. Vuckovic, and F. Wang, "Electrical control of silicon photonic crystal cavity by graphene," Nano Lett. **13**(2), 515–518 (2013).
21. Z. L. Lu and W. S. Zhao, "Nanoscale electro-optic modulators based on graphene-slot waveguides," J. Opt. Soc. Am. B **29**(6), 1490–1496 (2012).
22. C. Manolatou, M. J. Khan, S. H. Fan, P. R. Villeneuve, H. A. Haus, and J. D. Joannopoulos, "Coupling of modes analysis of resonant channel add-drop filters," IEEE J. Quantum Electron. **35**(9), 1322–1331 (1999).
23. C. Qiu, J. Chen, Y. Xia, and Q. Xu, "Active dielectric antenna on chip for spatial light modulation," Sci. Rep. **2**, 855 (2012).
24. M. Xu, F. Li, T. Wang, J. Y. Wu, L. Y. Lu, L. J. Zhou, and Y. K. Su, "Design of an electro-optic modulator based on a silicon-plasmonic hybrid phase shifter," J. Lightwave Technol. **31**(8), 1170–1177 (2013).
25. P. Dong, S. Liao, D. Feng, H. Liang, D. Zheng, R. Shafiiha, C. C. Kung, W. Qian, G. Li, X. Zheng, A. V. Krishnamoorthy, and M. Asghari, "Low V-pp, ultralow-energy, compact, high-speed silicon electro-optic modulator," Opt. Express **17**(25), 22484–22490 (2009).
26. D. J. Thomson, F. Y. Gardes, J. M. Fedeli, S. Zlatanovic, Y. Hu, B. P. P. Kuo, E. Myslivets, N. Alic, S. Radic, G. Z. Mashanovich, and G. T. Reed, "50-Gb/s silicon optical modulator," IEEE Photonics Technol. Lett. **24**(4), 234–236 (2012).
27. C. T. Phare, Y. H. D. Lee, J. Cardenas, and M. Lipson, "Graphene electro-optic modulator with 30 GHz bandwidth," Nat. Photonics **10**, 1038 (2015).

1. Introduction

Large-scale integration of nanoscale electro-optic (EO) modulators with high efficiencies and speeds has become increasingly important for optical communication systems [1, 2]. Silicon-based EO modulators show merits regarding device footprints, modulation speeds, power consumptions, and mass-productivity. However, the weak EO effect of silicon still sets a technical bottleneck for these devices [3], motivating the development of modulators with new materials. The introduction of graphene as an active medium has attracted a lot of attentions due to its high carrier mobility [4] and gate-controllable broadband absorption [5]. To date, several prototype graphene-silicon hybrid EO modulators have been realized by integrating graphene with silicon waveguides or micro-ring resonators (MRRs) [6–9]. The waveguide-based modulators require graphene-silicon interaction lengths on the order of several tens of micrometers [6, 7], resulting in large device footprints and high power consumptions. For MRR-based modulators [8, 9], enhanced light-matter interactions in the resonant cavities lead to increased modulation efficiencies and reduced device footprints. Nevertheless, they present limited free spectral ranges (FSRs). The multiple resonances of a modulator may affect neighboring channels, thus are being undesired in the wavelength-division multiplexed (WDM) systems [10]. Although the FSR of a MRR can be increased to a certain extent by reducing the circumference, it results in increased bending loss and decreased quality factor (Q-factor), which increases the power consumption and degrades the modulation efficiency [11].

In this paper, a novel EO modulator for WDM systems based on a graphene-silicon hybrid structure is proposed and numerically studied. The proposed structure combines the merits of a 1D photonic crystal nanobeam (PCN) cavity and graphene in a single device. Compared to a MRR, the PCN cavity can achieve an ultra-compact device footprint while still retaining a relatively high Q-factor [12, 13], which is critical for low-power and high-efficiency operation. The ultra-compact footprint leads to high integration density and significantly increased FSR. The large FSR is especially attractive for integrated WDM systems since it offers a single resonance in an ultra-wide band without being affected by adjacent resonances of the device [11]. Through electrically tuning the Fermi level of the graphene, both the Q-factor and resonant wavelength of the PCN cavity can be strongly changed, whereby the in-

#242279 Received 8 Jun 2015; revised 31 Jul 2015; accepted 31 Jul 2015; published 27 Aug 2015

plane lightwave can be efficiently modulated [8]. Benefiting from the ultrafast and strong EO effect of the graphene and from the enhanced light-matter interaction of the graphene-silicon hybrid PCN cavity design, high-speed and high-ER lightwave modulation can thus be achieved in a wide spectral window. Finite-difference time-domain (FDTD) simulation results show that our proposed modulator can provide a large FSR of 125.6 nm, a high modulation speed of 133 GHz, and a modulation depth greater than 10 dB in a small mode volume.

2. Device structure and operation principle

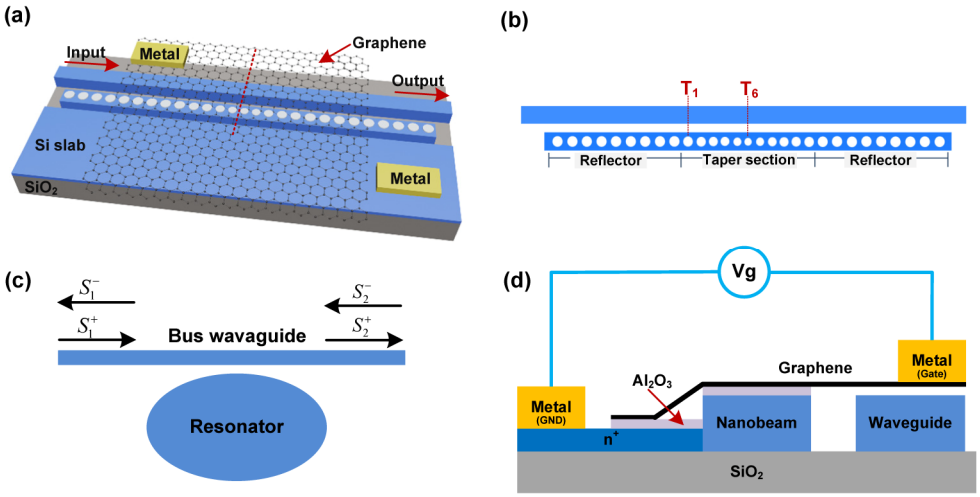

Fig. 1. (a) Schematic perspective view of the proposed EO modulator. Note that there is no graphene covering the air holes of the PCN cavity. (b) Top-view of the PCN cavity. The PCN cavity is symmetric with respect to its center. (c) The model of the PCN cavity as a single-mode optical resonator coupled with a bus waveguide. (d) The cross-section of the proposed device corresponding to the red dashed line in (a).

The proposed modulator is schematically visualized in Fig. 1(a), which consists of a graphene-silicon hybrid PCN cavity side-coupled to a bus waveguide. The top view of the PCN cavity containing reflectors and taper section is illustrated in Fig. 1(b). To achieve a high *Q*-factor and a large FSR within a small mode volume, the structural parameters of the PCN cavity listed in Table 1 are designed according to Refs [13–15]. The reflector with nine holes guarantees that the light is highly reflected within the telecommunication band, and the taper section is designed to smoothen the reflected optical response and to provide a single resonance within a large spectral window of high reflectivity. As the PCN cavity is symmetric with respect to its center, the taper section parameters are shown for half length of the cavity. The parameters of the reflectors and taper section are designed with respect to a length constant *L*.

As shown in Fig. 1(c), the PCN cavity can be modeled as a single-mode optical resonator coupled with a bus waveguide. In order to achieve a relatively high *Q*-factor and a large extinction ratio (ER), the coupling gap and *L* are optimized to be 167 nm and 452.5 nm, respectively. As shown in Fig. 1(d), the PCN cavity is not doped to achieve a high *Q*-factor. Since the n-doped region on the slab is very close to the PCN cavity with a gap of 1.5 μm, the Fermi level of the graphene on top of the PCN cavity can be efficiently tuned through electrical gating [8]. Through electrically tuning of the Fermi level, both the loss and the resonant wavelength of the PCN cavity can be changed, which can in turn modulate the in-plane travelling wave transmitted in the bus waveguide.

#242279 Received 8 Jun 2015; revised 31 Jul 2015; accepted 31 Jul 2015; published 27 Aug 2015

Table 1. Designed structural parameters of the PCN cavity

Cavity	Cavity width	Waveguide width	Coupling gap	Height
	500 nm	500 nm	167 nm	220 nm
Mirror section	Length constant	Hole diameter	Distance between holes	
	L = 452.5 nm	L/2	(0.9)L	
Taper section	Hole	Diameter (nm)	Distance between holes	
	T_1	(L/2)(0.98)	(L)(0.9)(0.98)	
	T_2	(L/2)(0.92)	(L)(0.9)(0.92)	
	T_3	(L/2)(0.88)	(L)(0.9)(0.88)	
	T_4	(L/2)(0.84)	(L)(0.9)(0.84)	
	T_5	(L/2)(0.80)	(L)(0.9)(0.80)	
	T_6	(L/2)(0.76)	(L)(0.9)(0.76)	

The proposed modulator can be fabricated through standard semiconductor fabrication processes. An n-type doping region is formed by patterned ion implantation in the 50-nm-thick silicon slab. 7-nm-thick Al_2O_3 as the gate dielectric material is deposited on part of the silicon slab, on the bus waveguide, and on the PCN cavity, after which the chemical vapor deposition (CVD) prepared graphene sheet is transferred onto the Al_2O_3 layer. Following these steps, E-beam lithography (EBL) is used to define the device pattern, which is then etched into the silicon layer by inductively coupled plasma (ICP) etching. Finally, metal electrodes are deposited by lithography and lift-off process, making contacts to the bottom n-type doped silicon slab and the graphene sheet. The footprint of the PCN cavity can be possibly down to ~20 μm^2 [15].

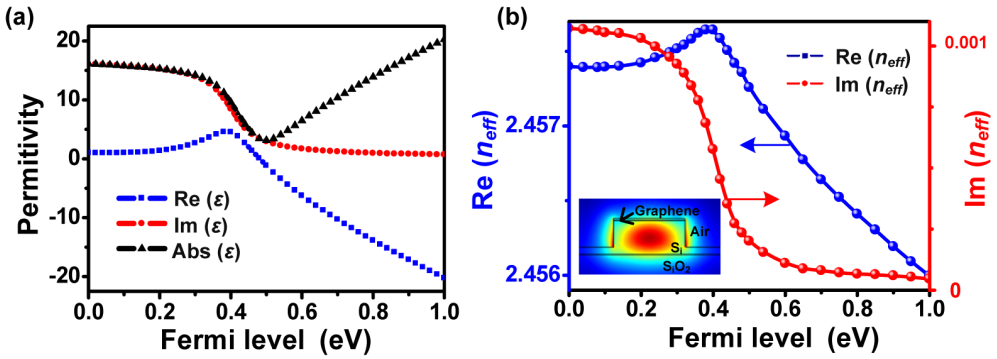

Fig. 2. (a) Real part, imaginary part, and magnitude of the calculated anisotropic in-plane permittivity of graphene under different Fermi levels. (b) The real and imaginary parts of effective modal index of 500 × 220 nm^2 single-mode silicon waveguide with graphene on top as a function of the Fermi level. The inset is the electric field distribution profile of the TE mode. All the simulations are performed at an operation wavelength of 1550 nm.

The graphene sheet serves as a variable-index optical cladding upon the top surface of the PCN waveguide core. This cladding overlaps with fringing fields of the TE_0 mode, and the light in the silicon core is evanescently coupled to the graphene layer and about ~0.09% of the total power is located in the sheet of graphene. By employing a waveguide structure with embedded graphene layers in the silicon waveguide core [16], increased power ratio and effective index variation can be achieved. In our design, the graphene layer is transferred onto the PCN cavity to simplify the fabrication process. We illustrate the modulation principle of

#242279 Received 8 Jun 2015; revised 31 Jul 2015; accepted 31 Jul 2015; published 27 Aug 2015

the proposed device by starting with gate-controllable permittivity of graphene. The anisotropic permittivity of graphene is taken into account in the simulations. The surface-normal component of permittivity $\varepsilon_{\perp}$ is set to be a constant of 2.5 based on the dielectric constant of graphene [9, 17]. The relationship between the in-plane permittivity of the graphene and the Fermi level is studied by using the random phase approximation and the Kramers-Kronig relation [18]. The imaginary part $\varepsilon_g^{"}$ is characterized by the absorption of interband transitions and intraband transitions, whereas the real part $\varepsilon_g^{'}$ can be obtained from the Kramers-Kronig relation as follows [18]:

$$\varepsilon_g^{'}(E_f) = 1 + \frac{e^2}{8\pi E_p \varepsilon_0 d} \ln \frac{(E_p + 2|E_f|)^2 + \Gamma^2}{(E_p - 2|E_f|)^2 + \Gamma^2} - \frac{e^2}{\pi \varepsilon_0 d} \frac{|E_f|}{{E_p}^2 + (1/\tau)^2}, \tag{1}$$

$$\begin{aligned} \varepsilon_g^{"}(E_f) = {} & \frac{e^2}{4E_p \varepsilon_0 d}\left[1 + \frac{1}{\pi}\left(\tan^{-1}\frac{E_p - 2|E_f|}{\Gamma} - \tan^{-1}\frac{E_p + 2|E_f|}{\Gamma}\right)\right] \\ & + \frac{e^2}{\pi\tau E_p \varepsilon_0 d} \frac{|E_f|}{E_p^2 + (1/\tau)^2}, \end{aligned} \tag{2}$$

where d = 1 nm is the thickness of the graphene sheet [19, 20]. Γ is the interband transition broadening estimated to be 110 meV from the graphene reflection spectrum [18], and $1/\tau$ is the free carrier scattering rate set to zero in our simulations since it has negligible influence on the dielectric constant at the incident photon frequency ω. E_p represents the photon energy at the wavelength of 1550 nm. The relation between the Fermi level and the in-plane permittivity of the graphene is depicted in Fig. 2(a). Note that the permittivity of graphene varies quickly with a dip in the magnitude curve corresponding to E_f = 0.51 eV, where "dielectric graphene" changes to "metallic graphene" [21], indicating high modulation capability. The variation of the permittivity has strong influence on the effective index of the graphene-silicon hybrid waveguide. As shown in Fig. 2(b), the effective mode index n_{eff} of the 500 × 220 nm^2 single-mode waveguide with graphene on top is calculated from the eigen-mode solver of the commercial software COMSOL, and the inset shows the electric field distribution for the transverse electric (TE) mode. The variation trend of the effective mode index as shown in Fig. 2(b) is similar to that of the graphene's permittivity in Fig. 2(a). The maximum value at E_f = 0.4 eV and the minimum value at E_f = 1 eV of Re(n_{eff}) experience an effective index change of 0.00164. This value of Δn_{eff} has been significantly enhanced compared with that of the conventional optical modulators on the order of 10^{-4} [3, 9]. Since the real part of n_{eff} is the determining factor for the resonant wavelength, while the imaginary part determines the quality factor of the cavity mode, both the resonant wavelength and the quality factor of the cavity mode can thus be changed by electrically tuning of the Fermi level of the graphene.

3. Simulation results and discussions

FDTD simulations are performed to numerically study the performances of the proposed modulator. The mesh size inside the graphene sheet is set to 0.05 nm, and it gradually increases outside the graphene sheet. Figure 3(a) shows the normalized transmission spectra of the device at varied Fermi levels. Off-resonance, about 98% of the light is transmitted. On resonance, with the increasing of E_f, the loss caused by the graphene decreases, thus approaching the critical coupling condition with higher Q-factor and larger ER. A single resonance within a broad operation band ranging from 1.4 to 1.67 μm at E_f = 0.9 eV is shown in Fig. 3(b). A FSR as large as 125.6 nm, a high ER of ~14 dB, and a relatively high Q-factor of ~5000 are achieved in our proposed device. If the Fermi level is shifted from 0.4 eV to 0.9 eV, the real part of n_{eff} experiences a change of 0.0164 as shown in Fig. 2(b), leading to a 0.95-nm resonance blue shift as plotted in Fig. 3(c). It should be noted that the change of the

#242279 Received 8 Jun 2015; revised 31 Jul 2015; accepted 31 Jul 2015; published 27 Aug 2015

Fermi level also leads to increased Q-factor, which can be attributed to the decreased imaginary part of n_{eff}. As depicted in Fig. 3(e), the modulation depth is as large as ~12.5 dB at λ = 1549.29 nm.

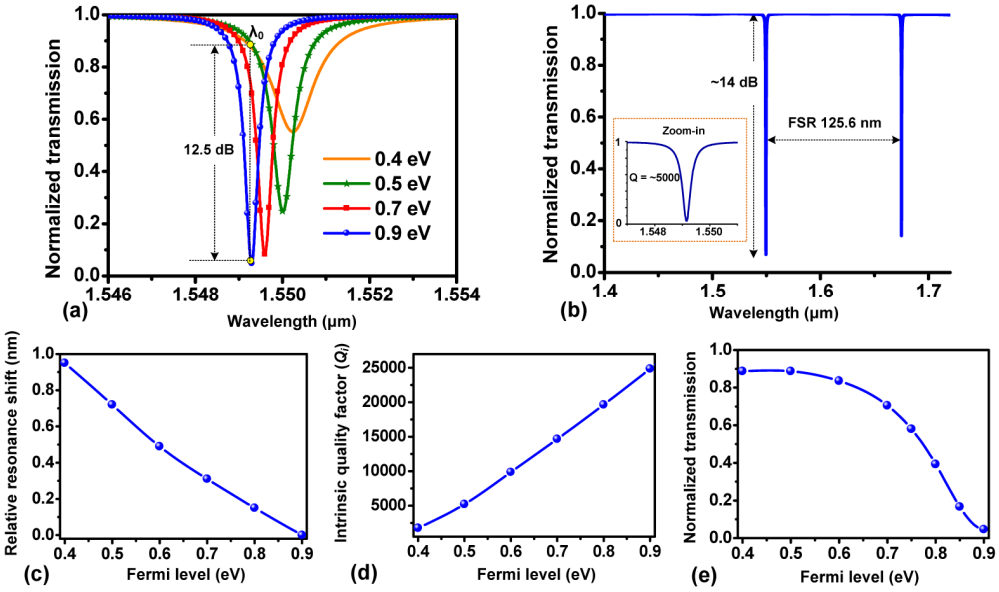

Fig. 3. (a) Normalized transmission spectra of the proposed device at different Fermi levels. (b) Normalized transmission spectrum ranging from 1400 nm to 1670 nm at E_f = 0.9 eV. Inset shows zoom-in view of the spectrum ranging from 1545 nm to 1553 nm. (c) Relative resonance wavelength shift defined as the resonance wavelength detuning from the resonance wavelength at E_f = 0.9 eV. (d) Calculated intrinsic quality factor. (e) Normalized transmission at 1549.3 nm.

We also use the analytic model to extract the parameters of the proposed device under different Fermi levels of the graphene. The spectra obtained from FDTD simulations agree well with those calculated from the analytical model based on the coupled mode theory and the transfer matrix method. If the PCN cavity on a silicon-on-insulator (SOI) substrate is modeled as the optical resonator in Fig. 1(c), the equations for the evolution of the resonator mode in time can be written as [22, 23]:

$$\frac{da}{dt} = [j(\omega - \omega_0) - \frac{1}{2\tau_0} - \frac{|\kappa_1|^2 + |\kappa_2|^2}{2}]a + k_1 S_1^+ , \quad (3)$$

$$S_2^+ = S_1^+ - \kappa_1^* a , \quad (4)$$

where $j = \sqrt{-1}$, ω and ω_0 are the frequency of the input wave in the bus waveguide and the resonant frequency of PCN cavity, respectively. S_1^+ and S_2^+ denote the amplitudes of the input and output waves, respectively. The squared magnitudes of S_1^+ and S_2^+ are equal to the powers of the input and output waves, respectively. The amplitude of the resonant mode is described by a, and $|a|^2$ is normalized as the energy in the cavity. τ_0 is the intrinsic photonic lifetime of the cavity. τ_0 is related to the intrinsic quality factor Q_i as $\tau_0 = Q_i \lambda_0/2\pi c$, with c denoting the light speed in vacuum. κ_1 and κ_2 are the coupling coefficients associated with the forward and backward propagating waves in the bus waveguide. The coupling quality factor Q_c is determined by the coupling coefficients as $|\kappa_1|^2 + |\kappa_2|^2 = 2\pi c/Q_c \lambda_0$. Under the steady state, i.e., $da/dt = 0$, the amplitude of the resonant mode can be expressed as

#242279 Received 8 Jun 2015; revised 31 Jul 2015; accepted 31 Jul 2015; published 27 Aug 2015

$$a = \frac{k_1 S_1^+}{-i(\omega - \omega_0) + (|\kappa_1|^2 + |\kappa_2|^2)/2 + 1/2\tau_0} , \quad (5)$$

Substituting a from Eq. (5) into Eqs. (3) and (4), the transmission of the modeled resonator T can be obtained as

$$T = \frac{|S_2^+|^2}{|S_1^+|^2} = \frac{Q_c^2 \lambda^2 + [2Q_i Q_c(\lambda - \lambda_0)]^2}{(Q_c + Q_i)^2 \lambda^2 + [2Q_i Q_c(\lambda - \lambda_0)]^2} , \quad (6)$$

The simulated spectra are fitted by T in Eq. (6) using OriginPro 8 (Origin Lab Inc.), then Q_c and Q_i with minimum discrepancy between the two spectra can be obtained. If the Fermi level of the graphene is tuned from 0.4 eV to 0.9 eV, Q_i increases from ~1700 to ~25,000 as illustrated in Fig. 3(d), and Q_c (~5000) is not changed much as expected, suggesting that the loss from the graphene determines the bandwidth of the resonance notch.

The external applied voltage V_g used to tune the Fermi level of the graphene can be related to E_f by the formula [18]:

$$E_f = \hbar V_f \sqrt{\pi(n_0 + \frac{C_p |V_g|}{q})} , \quad (7)$$

where C_p is the effective capacitance per unit area estimated to be ~20 mF/m^2 for the proposed device [20]. $V_f = 10^6$ m/s is the Fermi velocity for the graphene, and $n_0 = 1.17 \times 10^{17}$ m^{-3} is the intrinsic carrier concentration [8]. Thus $V_g = 6.4$ V is needed to shift E_f from 0.4 eV to 0.9 eV. The modulation speed of the proposed modulator is intrinsically determined by the RC time constant. The contact resistance R of our proposed device is estimated to be ~20 Ω [8] and the total capacitance C is assumed to be ~60 fF [23]. Hence, the modulation speed is calculated to be $1/2\pi RC$ = ~133 GHz [24], which could be much higher than those of conventional silicon EO modulators based on free-carrier plasma dispersion effect [25]. The modulator draws electric current only during the extremely brief charging and discharging times. For comparisons, Table 2 summarizes some state-of-the-art silicon-based EO modulators in term of several key parameters.

Table 2. Comparison with state-of-the-art silicon-based EO modulators

Description	Device footprint	Bias voltage	Modulation speed	Extinction ratio	Energy consumption	Ref.
PCN cavity with micro-heater	20 μm^2	~0.1 V	~10 KHz	~10 dB	~0.5 J/bit	[15]
PN depletion microring	1000 μm^2	–1 V	11 GHz	6.5 dB	50 fJ/bit	[25]
PN depletion MZM	~10^4 μm^2	–4 V	50 GHz	3.1 dB	4.2 pJ/bit	[26]
Graphene-silicon waveguide	25 μm^2	–3.5 V	1.2 GHz	~3.6 dB	0.67 pJ/bit	[6]
Graphene-Si_3N_4 microring	~5000 μm^2	–30 V	22 GHz	~10 dB	0.8 pJ/bit	[27]
Our device (Simulation)	20 μm^2	–6.4 V	133 GHz	12.5 dB	0.6 pJ/bit	–

#242279 Received 8 Jun 2015; revised 31 Jul 2015; accepted 31 Jul 2015; published 27 Aug 2015

4. Conclusion

In conclusion, we have proposed and numerically demonstrated a compact high-speed EO modulator based on a silicon PCN cavity with gated graphene on top. The resonance wavelength and *Q*-factor can be controlled by electrically tuning the Fermi level of the graphene, providing an efficient method to achieve light modulation at the telecommunication band. Simulation results show that the proposed modulator can provide a large FSR up to 125.6 nm, a high modulation depth of 12.5 dB, and a high modulation speed of 133 GHz. The compact footprint, CMOS compatibility and excellent modulation performance may open new opportunities for applications in future chip-integrated interconnects and ultrahigh-speed WDM optical communication systems.

Acknowledgments

This research was supported in part by the National Natural Science Foundation of China under Grant 61125504/61235007, in part by the 863 High-Tech Program under Grant 2015AA015503/2015AA017001, and in part by the Natural Science Foundation of Shanghai under Grant 15ZR1422800. R.S. acknowledges support of the AFOSR on grant FA9660-13-1-0196 and of the UK EPSRC on Project Migration.

#242279 Received 8 Jun 2015; revised 31 Jul 2015; accepted 31 Jul 2015; published 27 Aug 2015